Research in Astronomy and Astrophysics, 25:014002 (11pp), 2025 January

https://doi.org/10.1088/1674-4527/ada3b5
CSTR: 32081.14.RAA.ada3b5

The FAST Galactic Plane Pulsar Snapshot Survey. VII. Six Millisecond Pulsars in Compact Orbits with Massive White Dwarf Companions

Z. L. Yang[1,2], J. L. Han[1,2,3], T. Wang[1], P. F. Wang[1,2,3], W. Q. Su[1,2], W. C. Chen[4], C. Wang[1,2,3], D. J. Zhou[1], Y. Yan[1,2], W. C. Jing[1,2], N. N. Cai[1], L. Xie[1], J. Xu[1,3], H. G. Wang[5,6], and R. X. Xu[7]
[1] National Astronomical Observatories, Chinese Academy of Sciences, Beijing 100101, China; hjl@nao.cas.cn
[2] School of Astronomy and Space Science, University of Chinese Academy of Sciences, Beijing 100049, China
[3] Key Laboratory of Radio Astronomy and Technology, Chinese Academy of Sciences, Beijing 100101, China
[4] School of Science, Qingdao University of Technology, Qingdao 266525, China
[5] Department of Astronomy, School of Physics and Materials Science, Guangzhou University, Guangzhou 510006, China
[6] National Astronomical Data Center, Greater Bay Area, Guangzhou 510006, China
[7] Department of Astronomy, Peking University, Beijing 100871, China
Received 2024 September 23; revised 2024 November 29; accepted 2024 December 20; published 2025 January 31

Abstract

Binary millisecond pulsars with a massive white dwarf (WD) companion are intermediate-mass binary pulsars (IMBPs). They are formed via the Case BB Roche-lobe overflow evolution channel if they are in compact orbits with an orbital period of less than 1 day. They are fairly rare in the known pulsar population; only five such IMBPs have been discovered before, and one of them is in a globular cluster. Here we report six IMBPs in compact orbits: PSRs J0416+5201, J0520+3722, J1919+1341, J1943+2210, J1947+2304 and J2023+2853, discovered during the Galactic Plane Pulsar Snapshot survey by using the Five-hundred-meter Aperture Spherical radio Telescope, doubling the number of such IMBPs due to the high survey sensitivity in the short survey time of 5 minutes. Follow-up timing observations show that they all have either a CO WD or an ONeMg WD companion with a mass greater than about 0.8 $M_{\odot}$ in a very circular orbit with an eccentricity in the order of $\lesssim 10^{-5}$. PSR J0416+5201 should be an ONeMg WD companion with a remarkable minimum mass of 1.28 $M_{\odot}$. These massive WD companions lead to a detectable Shapiro delay for PSRs J0416+5201, J0520+3722, J1943+2210, and J2023+2853, indicating that their orbits are highly inclined. From the measurement of the Shapiro delay, the pulsar mass of J1943+2210 was constrained to be $1.84^{+0.11}_{-0.09}$ $M_{\odot}$, and that of PSR J2023+2853 to be $1.28^{+0.06}_{-0.05}$ $M_{\odot}$.

Key words: (stars:) binaries (including multiple): close – stars: evolution – (stars:) pulsars: general

1. Introduction

Binary millisecond pulsars (MSPs) with a CO/ONeMg white dwarf (WD) companion are intermediate-mass binary pulsars (IMBPs), because they have a more massive companion (see Figure 1) compared to these low-mass binary pulsars with a He WD companion with a mass less than 0.46 $M_{\odot}$ (Tauris & van den Heuvel 2023). When the WD companion has a mass of $\gtrsim$1.05 $M_{\odot}$, it must be an ONeMg WD. The CO WDs have a mass roughly in the range of 0.46–1.05 $M_{\odot}$. The IMBP systems are descendants of intermediate-mass X-ray binaries (IMXBs) where mass is transferred from a more massive donor to a less massive neutron star (NS). The most widely accepted explanation for the high spin frequencies of MSPs is the accretion of mass and angular momentum in a binary system (Alpar et al. 1982; Radhakrishnan & Srinivasan 1982; Bhattacharya & van den Heuvel 1991). The spin periods are therefore closely related to the amount of accreted mass in this process and, hence, provide constraints on the accretion process (Tauris et al. 2011, 2012). The mass transfer process can be dynamically unstable, leading to the formation of a common envelop (CE), which experiences much more complicated and unclear evolution depending on the mass of the donor star (Paczynski 1976; Iben & Livio 1993; Ivanova et al. 2013; Tauris & van den Heuvel 2023). During the H-shell burning phase, the donor star with a mass of 2–10 $M_{\odot}$ expands and enters the red giant branch. At the start of mass transfer, if the donor star is near the tip of the red giant branch and the merger can be avoided, an unevolved helium star will be left and then the post-CE orbital period will be $\leqslant$0.5 days (Tauris et al. 2012). The helium star will expand during the helium shell burning phase, leading to a new mass transfer called the Case BB Roche-lobe overflow (RLO; Tauris et al. 2011, 2012; Tauris & van den Heuvel 2023). An IMBP system can then be formed with a very tight orbit. During these mass transfer phases, the NS accretes only a little mass from its companion and is only mildly recycled.

Timing observations of binary MSPs provide an effective approach to studying IMBPs. The Keplerian binary parameters can be determined with a few observations (Freire et al. 2001; Bhattacharyya & Nityananda 2008), then the companion mass

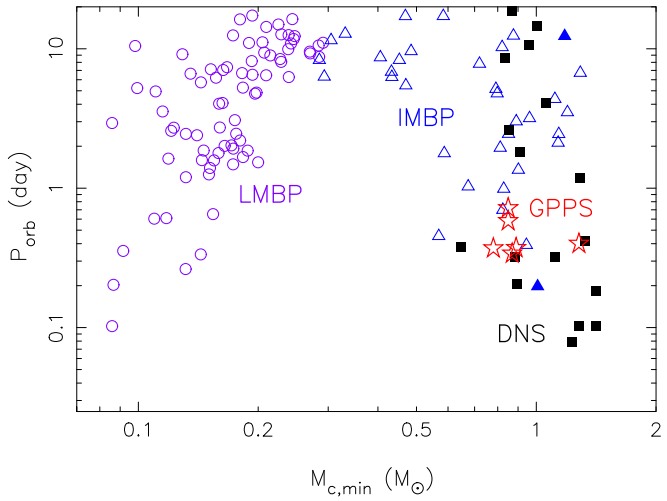

Figure 1. Six IMBPs (stars) in this paper are plotted among pulsars with a degenerate companion in the distribution of orbital period and minimum companion mass. The companions of low-mass binary pulsars (LMBP, circles) are He WDs, while the intermediate-mass binary millisecond pulsars (IMBP, triangles) have a CO/ONeMg WD companion. Pulsars in double neutron star (DNS) binary systems are marked by black filled squares. Binaries with an orbital eccentricity greater than 0.01 are marked with filled symbols. The minimum companion mass is derived from the mass function, assuming a pulsar mass of 1.4 $M_\odot$. Parameters are taken from the ATNF pulsar catalog (Manchester et al. 2005) (web version on 2024 September 27th), except for six IMBPs from this paper.

can be estimated based on the mass function. If any post-Keplerian (PK) binary parameters are precisely measured, then the masses of the pulsar and the WD companion can be better constrained under the general relativity frame (Damour & Taylor 1992). The proper motions, if measurable from long-term timing, can tell us the natal kick of the pulsar obtained during the formation of the binary systems.

Using the Five-hundred-meter Aperture Spherical radio Telescope (FAST, Nan 2006; Nan et al. 2011) which is the most sensitive single-dish radio telescope in the world, we are carrying out the FAST Galactic Plane Pulsar Snapshot (GPPS) survey aiming at discovering pulsars within the Galactic latitude of $\pm 10^\circ$ of the FAST visible sky area (Han et al. 2021). The survey observations are made with four pointings to cover a sky patch of 0.1575 square degrees, with an integration time for each pointing of 300 s, which gives the sensitivity of a few μJy for pulsars in the millisecond range, improved by two orders of magnitude compared to previous surveys (see Figure 6 in Han et al. 2021). The FAST GPPS survey has already successfully discovered more than 750 new pulsars[8] (Han et al. 2025). Among them, there are more than 170 MSPs and about 116 pulsars are in binary systems (Wang et al. 2025). The high sensitivity of FAST in such a short integration time is good at detecting pulsars in compact orbits. Here we report the timing

[8] http://zmtt.bao.ac.cn/GPPS/GPPSnewPSR.html

Table 1
Intermediate-mass Binary Millisecond Pulsars in Compact Circular Orbits of $P_{orb} < 1$ day and $e < 0.01$, Six are from this Paper and Five are Previously Known

PSR name	P (ms)	P_{orb} (days)	x (lt-s)	$M_{c,min}$ ($M_\odot$)	Reference
J1947+2304	10.89	0.339	2.40	0.87	(0)
J1919+1341	11.66	0.370	2.34	0.78	(0)
J1943+2210	12.87	0.372	2.58	0.89	(0)
J1748−2446N	8.667	0.386	1.62	0.48	(1)
J1952+2630	20.73	0.392	2.80	0.94	(2)
J0416+5201	18.24	0.396	3.51	1.28	(0)
J1757−5322	8.870	0.453	2.09	0.57	(3)
J0520+3722	7.913	0.580	3.37	0.85	(0)
J1802−2124	12.65	0.699	3.72	0.82	(4)
J2023+2853	11.33	0.718	4.00	0.89	(0)
J1525−5545	11.36	0.990	4.71	0.83	(5)

References: (0): this paper; (1): Ransom et al. (2005); (2): Knispel et al. (2011); (3): Edwards & Bailes (2001); (4): Faulkner et al. (2004); (5): Ng et al. (2014).

results of six binary pulsars: PSRs J0416+5201, J0520+3722, J1919+1341, J1943+2210, J1947+2304, and J2023+2853, with a companion more massive than 0.8 $M_\odot$. Because their orbits are nearly circular with a period of less than 1 day and ellipticity on the order of 10^{-5}, they must be IMBPs with either a CO WD or an ONeMg WD, with the parameter space mixed with double NSs (see Figure 1). The new discovery of six pulsars by the GPPS survey significantly enlarges the number of IMBPs in compact orbits (see Table 1).

The structure of the rest of this paper is arranged as follows: In Section 2, we describe the FAST observations of these pulsars, followed by the details of data analyses including the orbital parameter determination and pulsar timing. The detailed results of these six pulsars are presented in Section 3. The implications of our results and future prospects are discussed in Section 4.

2. FAST Observations and Data Reduction

All FAST observations have been carried out by using the *L*-band 19-beam receiver, covering a 500 MHz bandwidth centered at 1.25 GHz (Jiang et al. 2020). The data were recorded for 2 or 4 polarization channels, with a sampling time of 49.152 μs for all 2048 or 4096 frequency channels. Before or after every observation session, the calibration noise signals with a modulated amplitude of 1.1 K and a period of 2.01326 s are injected into the receiver feeds so that polarization data can be calibrated (Han et al. 2021; Wang et al. 2023).

The six IMBPs, PSRs J0416+5201, J0520+3722, J1919+1341, J1943+2210, J1947+2304 and J2023+2853, were discovered during the FAST GPPS survey (Han et al. 2021, 2025). PSR J0416+5201 was discovered in a snapshot observation on 2023 January 3rd, and then confirmed in a

15 minute tracking observation on 2023 February 13th. Afterward, several follow-up observations were made and then the initial orbital parameters were determined. Similarly, PSR J0520+3722 was discovered from a snapshot observation on 2022 November 16th, and then confirmed in a 15 minute tracking observation on 2023 January 6th. PSR J1919+1341 was discovered from an observation on 2020 August 7th; PSR J1943+2210 was discovered from an observation on 2021 June 27th; PSR J1947+2304 was discovered from an observation on 2020 December 15th; PSR J2023+2853 was discovered from an observation on 2019 March 29th (Han et al. 2021).

For each pulsar, after a few observations were done with FAST, we de-dispersed the data, and then searched for the barycenter spin periods and accelerations of the pulsar using PRESTO (Ransom 2001). These data are plotted in a two-dimensional plane and form an ellipse so that the orbital period ($P_{\rm orb}$) and the projected semimajor axis (x) can be obtained from the plot directly (Freire et al. 2001).

With this initial orbital period, we performed a two-dimensional search of orbital period ($P_{\rm orb}$) and time of ending node passage ($T_{\rm ASC}$) to fit the observed periods of different epochs, which provided the intrinsic spin period of the pulsar P and refined the three orbital parameters $P_{\rm orb}$, x and $T_{\rm ASC}$ (Bhattacharyya & Nityananda 2008).

For timing analysis, first we folded pulsar profiles with the initial orbital parameters for data segments of 5 minutes each, using the package DSPSR (van Straten & Bailes 2011). The "times of pulse arrival" (TOAs) were then extracted from these folded pulsar profiles using the package PSRCHIVE, an Open Source C++ development library for the analysis of pulsar astronomical data (Hotan et al. 2004). We then calibrated the polarization with the injected calibration signals using the command "PAC" in PSRCHIVE, and removed radio frequency interference using the "2σCRF" method (Chen et al. 2023). The Faraday rotation measures (RMs) were then determined using "RMFIT" and then polarization data were RM-corrected using "PAM." The data of all frequency channels were then added to form profiles of four sub-bands. The profiles were compared to a frequency-average template produced by the command "PSRSMOOTH" or "PAAS," then finally TOAs were extracted from all these files by using the command "PAT."

3. FAST Timing Results

After FAST observations over the years, including data obtained during the FAST GPPS survey and also by free-applied FAST projects (see details in authors contributions), and following the method in Freire & Ridolfi (2018), we produced the phase-connected timing solutions of these systems (see Tables 2 and 3). Then, all data were refolded again to achieve better precision. If no dispersion measure (DM) variations are found, all frequency channels were summed together to obtain more precise TOAs. The timing residuals are presented in Figures 2 and 4. No systematic trends as a function of epoch or orbital phase can be seen in these plots. During the analyses, the solar system ephemeris DE436[9] was applied to correct the motion of the phase center of FAST relative to the barycenter of the solar system, while the motion of the pulsars was described using the ELL1 model (or ELL1k model for Shapiro delay parameters) (Lange et al. 2001; Edwards et al. 2006), which are the commonly used orbital models for low eccentricity orbits.

We also divided the FAST observation data of the 500 MHz bandwidth into four sub-bands and then refined DM and RM values. After final corrections, we get the final polarization profiles as shown in Figure 3. Linear polarizations of pulse profiles of PSRs J1919+1341 and J1947+2304 are not yet detected from available data. Discussions of polarization profiles and geometry are presented in Section 4.3. The distances of these pulsars are estimated from the DMs by using the electron-density models NE2001 (Cordes & Lazio 2002) and YMW16 (Yao et al. 2017). Based on the precise astronomic positions of these pulsars from timing observations, we searched for their optical counterparts in the Pan-STARRS1 image but yielded no result (Chambers et al. 2016).

Among the six pulsars, we get the Shapiro delay for PSRs J0416+5201, J0520+3722, J1943+2210 and J2023+2853, which indicates that they are in edge-on orbits. When the orbit of a pulsar is nearly circular, the Shapiro delay can be described by PK parameters $r \equiv Gm_{\rm c}/c^3$ and $s \equiv \sin i$ via

$$\Delta_{\rm s} = -2r \ln\{1 - s\cos[2\pi(\phi - \phi_{\rm o})]\}, \quad (1)$$

here $m_{\rm c}$ is the companion mass, i is the orbital inclination angle, ϕ is the orbital phase and $\phi_{\rm o}$ is the conjunction phase at $\phi = 0.25$. Together with the mass function,

$$f(m) = (4\pi^2/G)x^3/P_{\rm orb}^2 = (m_{\rm c}\sin i)^3/(m_{\rm p} + m_{\rm c})^2, \quad (2)$$

the observed Shapiro delay can constrain the pulsar mass $m_{\rm p}$, the companion mass $m_{\rm c}$, and the orbital inclination i.

In the following, we discuss the detailed timing results of six pulsars.

3.1. PSR J0416+5201

PSR J0416+5201 has a spin period of 18.2 ms. The pulse profile consists of the one-component main pulse and double-peak interpulse with a separation of about 180° in the rotation longitude (see Figure 3).

Assuming the pulsar mass of 1.4 $M_\odot$, the minimum companion mass, derived from mass function, should be 1.28 $M_\odot$, in the mass range of NSs, but such an NS companion is rebutted by the circular orbit with an eccentricity of only a few 10^{-5}. Only an ONeMg WD can have such a mass. On the other hand, a WD should have a mass less than the Chandrasekhar mass limit of $\sim$1.4 $M_\odot$. We therefore can conclude that the companion mass of PSR J0416

[9] https://naif.jpl.nasa.gov/pub/naif/JUNO/kernels/spk/de436s.bsp.lbl

Table 2
Parameters of PSRs J0416+5201, J0520+3722 and J1919+1341 Derived from FAST Observations

Parameter	PSR J0416+5201 (GPPS 0560)	PSR J0520+3722 (GPPS 0538)	PSR J1919+1341 (GPPS 0215)
Right ascension, R.A. (J2000)	04:16:27.27754(19)	05:20:13.56522(5)	19:19:23.0125(7)
Declination, decl. (J2000)	+52:01:25.774(4)	+37:22:09.573(7)	+13:41:09.29(1)
Galactic longitude, l (deg)	151.61631	170.03911	48.26673
Galactic latitude, b (deg)	0.95628	0.15093	0.15517
Spin frequency, ν (Hz)	54.822288789105(3)	126.370150421555(7)	85.79476748198(7)
Spin frequency derivative, $\dot{\nu}$ (Hz s^{-1})	$-7.001(16) \times 10^{-16}$	$-5.694(2) \times 10^{-15}$	$-1.25(2) \times 10^{-16}$
Reference epoch (MJD)	60300	60300	59393
Spin period, P (s)	0.018240556790575(9)	0.0079132611353561(4)	0.011655722479931(1)
Spin period derivative, $\dot{P}$ (s s^{-1})	$2.329(5) \times 10^{-19}$	$3.5653(15) \times 10^{-19}$	$1.70(3) \times 10^{-20}$
Characteristic age, τ_c (Gyr)	1.24	0.352	10.9
Dispersion measure (DM) (pc cm^{-3})	140.497(3)	88.9858(9)	394.56(1)
DM Distance from NE2001/YMW16 (kpc)	4.4/2.8	2.3/1.7	9.9/8.7
Faraday rotation measure, RM (rad m^{-2})	−196(3)	28(3)	…
Flux density at 1.25 GHz (μJy)	39.3(2)	128.0(4)	23.4(4)
Orbital period, P_{orb} (days)	0.39646949377(13)	0.57967552341(16)	0.3703382666(5)
Projected semimajor axis, x (lt-s)	3.505563(8)	3.372430(3)	2.34094(2)
Time of ascending node passage, T_{ASC} (MJD)	60317.56895079(5)	60298.52239671(5)	59392.5733017(8)
Mass function, $f(m)$ ($M_\odot$)	0.2942636(17)	0.1225580(3)	0.100429(2)
Minimum companion mass ($M_\odot$)	1.28	0.85	0.78
First Laplace parameter, $\epsilon_1 = e \sin\omega$	$2.2(3) \times 10^{-5}$	$2(2) \times 10^{-6}$	$0.8(1.8) \times 10^{-5}$
Second Laplace parameter, $\epsilon_2 = e \cos\omega$	$3.99(17) \times 10^{-5}$	$-1.0(1.3) \times 10^{-6}$	$0.7(1.2) \times 10^{-5}$
Sine of inclination angle, $\sin i$	0.988(8)	0.9980(14)	…
Companion mass, m_c ($M_\odot$)	1.7(5)	0.70(13)	…

Note. The timing results are obtained through the package TEMPO2 (Hobbs et al. 2006) with the ELL1k model, in units of TCB. The uncertainty of each TOA is scaled by T2EFAC to set the reduced χ^2 to 1. The uncertainty of the model parameters in brackets is the 68.3% confidence level (1σ uncertainty). The minimum companion mass is derived from the mass function assuming a pulsar mass of 1.4 $M_\odot$. The flux density at 1.25 GHz was calculated by using PSRFLUX in PSRCHIVE (Hotan et al. 2004) for the calibrated profiles.

+5201 is probably in the range of 1.28 and 1.4 $M_\odot$. Previously discovered pulsars with such massive WD companions are PSRs J1227−6208 ($1.21 < m_c/M_\odot < 1.47$; see Colom i Bernadich et al. 2024), J2222−0137 ($m_c = 1.319(4)$ $M_\odot$; see Guo et al. 2021), J1528−3146 ($m_c = 1.33^{+0.08}_{-0.07}$ $M_\odot$; see Berthereau et al. 2023), J1439−5501 ($m_c = 1.27^{+0.13}_{-0.12}$ $M_\odot$; see Jang et al. 2024) and B2303+46 ($1.2 < m_c/M_\odot < 1.4$; see van Kerkwijk & Kulkarni 1999), but none of them have a compact orbit like PSR J0416+5201. The massive companion in an orbital period of 0.396 days should merge with PSR J0416+5201 in about 3.1 Gyr.

We detected the Shapiro delay of the PSR J0416+5201 binary system, which implies an edge-on orbit. The companion mass is then further constrained by the Shapiro delay as being 1.7(5) $M_\odot$ (see Table 2), which provides an independent coarse but consistent mass constraint.

3.2. PSR J0520+3722

The phase-connected timing solution of this binary system has been obtained from the timing data over two years. Among six IMBPs, PSR J0520+3722 has the fastest spin period of 7.91 ms and the youngest characteristic age of 0.35 Gyr. Its pulse profile has a main pulse and an interpulse with a separation of about 180° in the rotation longitude (see Figure 3), with a clear circular polarization sense-reversal at the center of the two-peak main pulse.

The companion mass is constrained by the mass function of the binary and the Shapiro delay detected in timing data, as being 0.70(13) $M_\odot$, indicating that its companion is a CO WD. However, the precision of two measurable Shapiro delay parameters is not precise enough to constrain the pulsar mass. Assuming a pulsar mass of 1.4 $M_\odot$, the pulsar will merge with its companion after ∼12 Gyr.

3.3. PSR J1919+1341

PSR J1919+1341 is a mildly recycled pulsar with a spin period of 11.7 ms. PSR J1919+1341 has been frequently detected by the FAST L-band 19-beam receiver even when FAST is tracking PSRs J1918+1340g (GPPS0081) and PSR J1920+1340g (GPPS0423), though it is 1.′5 offset from the beam-center of one of the 19 beams. The TOAs have a large weighted root mean square (rms) timing residual of 85 μs due to the weaker pulse, the beam-offset, the wide pulse and also

Table 3
Same as Table 2 but for PSRs J1943+2210, J1947+2304, and J2023+2853

Parameter	PSR J1943+2210 (GPPS 0227)	PSR J1947+2304 (GPPS 0379)	PSR J2023+2853 (GPPS 0201)
Right ascension, R.A. (J2000)	19:43:53.77751(4)	19:47:28.938(1)	20:23:21.063406(6)
Declination, decl. (J2000)	+22:10:33.9676(8)	+23:04:15.30(1)	+28:53:41.4521(1)
Galactic longitude, l (deg)	58.512922	59.702179	68.944528
Galactic latitude, b (deg)	−0.852878	−1.120372	−4.809745
Proper motion in R.A. direction (mas yr^{-1})	−4.8(0.3)	⋯	−3.30(5)
Proper motion in decl. direction (mas yr^{-1})	−5.6(0.5)	⋯	−8.10(8)
Parallax (mas)	⋯	⋯	1.2(0.3)
Spin frequency, ν (Hz)	77.699600217448(5)	91.79624431818(6)	88.2697836893946(9)
Spin frequency derivative, $\dot{\nu}$ (Hz s^{-1})	$-3.4172(8) \times 10^{-16}$	$-3.39(7) \times 10^{-16}$	$-2.0898(1) \times 10^{-16}$
Reference epoch (MJD)	59800	59800	59262
Spin period, P (s)	0.0128700790892287(8)	0.010893691865365(7)	0.0113289050703785(1)
Spin period derivative, $\dot{P}$ (s s^{-1})	$5.6602(13) \times 10^{-20}$	$4.03(8) \times 10^{-20}$	$2.6821(2) \times 10^{-20}$
Characteristic age, τ_c (Gyr)	3.61	4.29	6.70
Dispersion measure (DM) (pc cm^{-3})	110.6643(10)	321.00(1)	22.75353(8)
DM Distance from NE2001/YMW16 (kpc)	4.6/4.0	9.8/10.2	2.0/1.6
DM derivative (pc cm^{-3} yr^{-1})	0.0013(6)	⋯	0.00017(4)
Faraday rotation measure, RM (rad m^{-2})	−37(3)	⋯	−65(3)
Flux density at 1.25 GHz (μJy)	25.0(1)	14.7(2)	662.5(2)
Orbital period, P_{orb} (days)	0.37205272916(4)	0.3388818158(7)	0.71823041855(1)
Projected semimajor axis, x (lt-s)	2.5798019(9)	2.39709(4)	4.0022204(3)
Time of ascending node passage, T_{ASC} (MJD)	59408.78530783(4)	59979.0730606(5)	59211.1878597(3)
Mass function, $f(m)$ ($M_\odot$)	0.13317810(13)	0.128777(7)	0.13343143(3)
Minimum companion mass, $m_{c,min}$ ($M_\odot$)	0.89	0.87	0.89
First Laplace parameter, $\epsilon_1 = e \sin\omega$	$-1.2(0.5) \times 10^{-6}$	$0.9(2.2) \times 10^{-5}$	$1.113(6) \times 10^{-5}$
Second Laplace parameter, $\epsilon_2 = e \cos\omega$	$-1.0(0.3) \times 10^{-6}$	$-1.4(1.6) \times 10^{-5}$	$0.694(5) \times 10^{-5}$
Rate of change of P_{orb}, $\dot{P}_{orb}$ (10^{-13} s s^{-1})	−1.3(0.7)	⋯	−0.9(0.3)
Rate of change of x, $\dot{x}$ (10^{-15} lt-s s^{-1})	⋯	⋯	−3(3)
Rate of periastron advance, $\dot{\omega}$	⋯	⋯	0.7(0.2)
Sine of inclination angle, $\sin i$	0.99979(5)	⋯	0.9939(4)
Companion mass, m_c ($M_\odot$)	1.03(3)	⋯	0.85(2)
Pulsar mass ($M_\odot$)	$1.84^{+0.11}_{-0.09}$	⋯	$1.28^{+0.06}_{-0.05}$
Companion mass ($M_\odot$)	$1.03^{+0.04}_{-0.03}$	⋯	$0.85^{+0.02}_{-0.02}$
Orbital inclination angle (deg)	$88.80^{+0.13}_{-0.14}$	⋯	$83.7^{+0.2}_{-0.3}$

Note. The Bayesian analyses have been carried out to get the pulsar and companion masses and the orbit inclination angle for the PSRs J1943+2210 and J2023+2853 which are binaries.

the relatively longer spin period. Assuming the pulsar mass is 1.4 $M_\odot$, the minimum mass of its companion is 0.78 $M_\odot$. Because of the very circular orbit, PSR J1919+1341 is probably circling a massive WD companion with an orbital period of 0.370 days. The merger timescale of this system is estimated to be 4.7Gyr. Large timing residuals prevent this system from having a good measurement of the Shapiro delay. Without any further constraints on the companion mass, its companion can be either a CO WD or an ONeMg WD.

3.4. PSR J1943+2210

After 3 yr of timing observations, we get the phase-coherent timing solution. PSR J1943+2210 has a spin period of 12.9 ms in a compact orbit with a period of 0.372 days and an eccentricity of $2.44(95) \times 10^{-6}$. The companion has a minimum mass of 0.89 $M_\odot$ according to the mass function. Based on all these measurements, we suggest that the companion should be a massive WD. The pulsar has a double-peak main pulse and a discrete one-peak secondary pulse with a rotation longitude separation of about 100°, so it is not the interpulse (see Figure 3).

We detected the proper motion of 7.4(0.5) mas yr^{-1}. Considering the DM distance of 4.6 kpc (Cordes & Lazio 2002) or 4.0 kpc (Yao et al. 2017), one can get the transverse velocity of $\sim 1.5 \times 10^2$ km s^{-1}, which is high but still reasonable (Shamohammadi et al. 2024). Combining the mass function of this binary system and the Shapiro delay (see Figure 5), we get the companion mass as being $1.03^{+0.04}_{-0.03}$ and an orbital inclination being $88.80^{+0.13}_{-0.14}$. The so-derived NS mass is

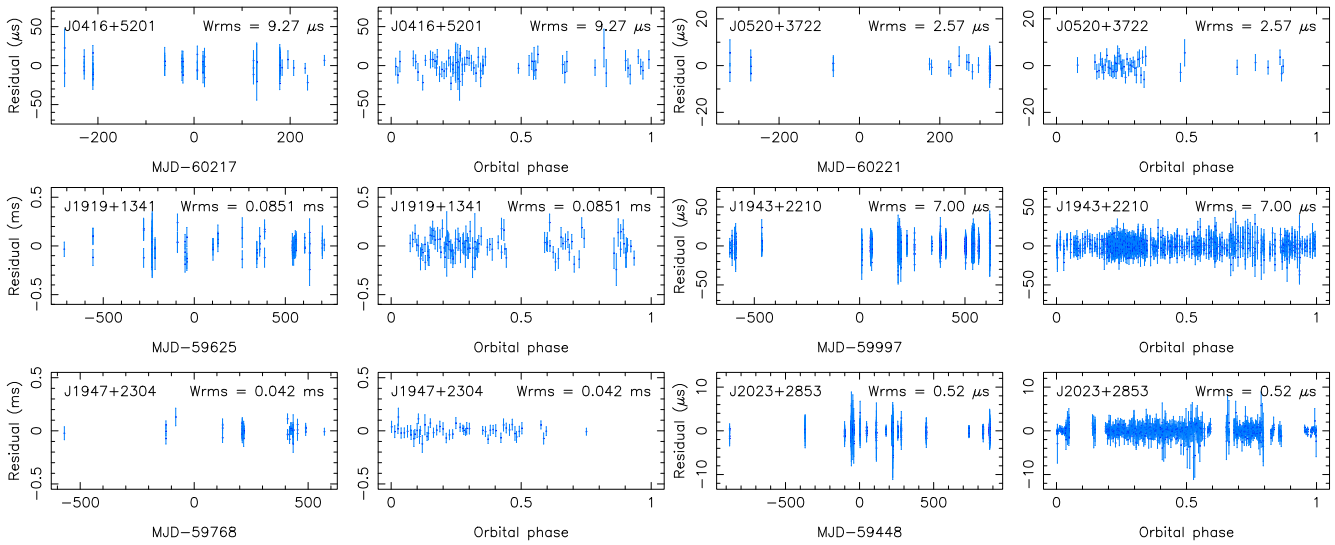

Figure 2. Timing residuals of the six pulsars measured by FAST, plotted along observation date in MJD and against the orbital phases. The differences between measured TOAs and the derived timing model, $W_{\rm rms}$, are marked in each panel.

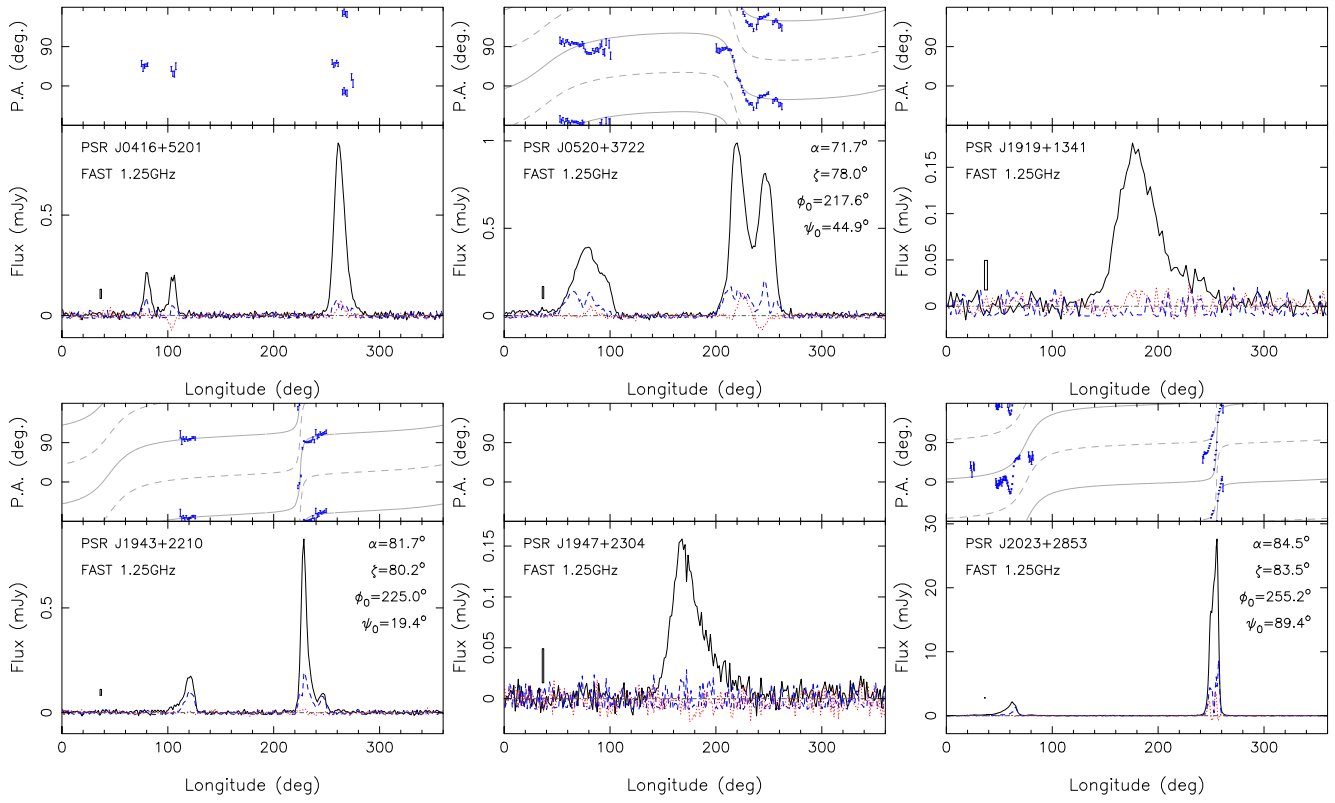

Figure 3. Polarization profiles of six pulsars. The total intensity profile (black line) and the linear (blue dashed line) and circular (red dotted line, positive for the left-hand sense) polarization profiles are plotted in the lower sub-panel with a scale-mark for $\pm 2\sigma$ and 1 bin-width, and the polarization angles (PA) are plotted in the upper sub-panel with the error bar for $\pm 1\sigma$. The best fitted PA curves by the rotating vector model (Radhakrishnan & Cooke 1969) for PSRs J1943+2210, J0520 +3722 and J2023+2853 are made with the "psrmodel" command in the PSRCHIVE tool package (Hotan et al. 2004) and shown by the gray lines, together with the orthogonal mode by the gray dashed lines. For PSRs J1919+1341 and J1947+2304, the RM and polarized emission cannot yet be determined from available data.

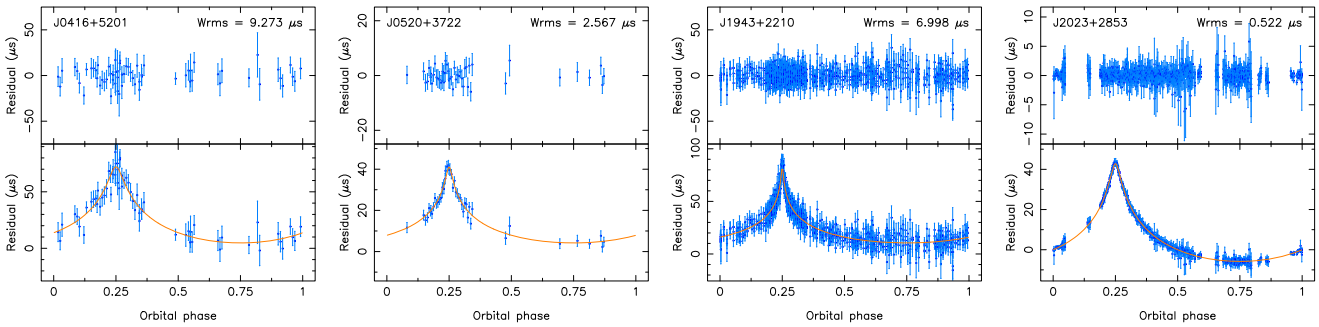

Figure 4. The detected Shapiro delay of PSRs J0416+5201, J0520+3722, J1943+2210 and J2023+2853 measured by FAST. In the upper sub-panels, the differences between measured TOAs and the derived timing model are marked against orbital phase. In the lower sub-panels, we display the timing residuals after the Shapiro delay is removed. All error bars represent $\pm 1\sigma$ uncertainty.

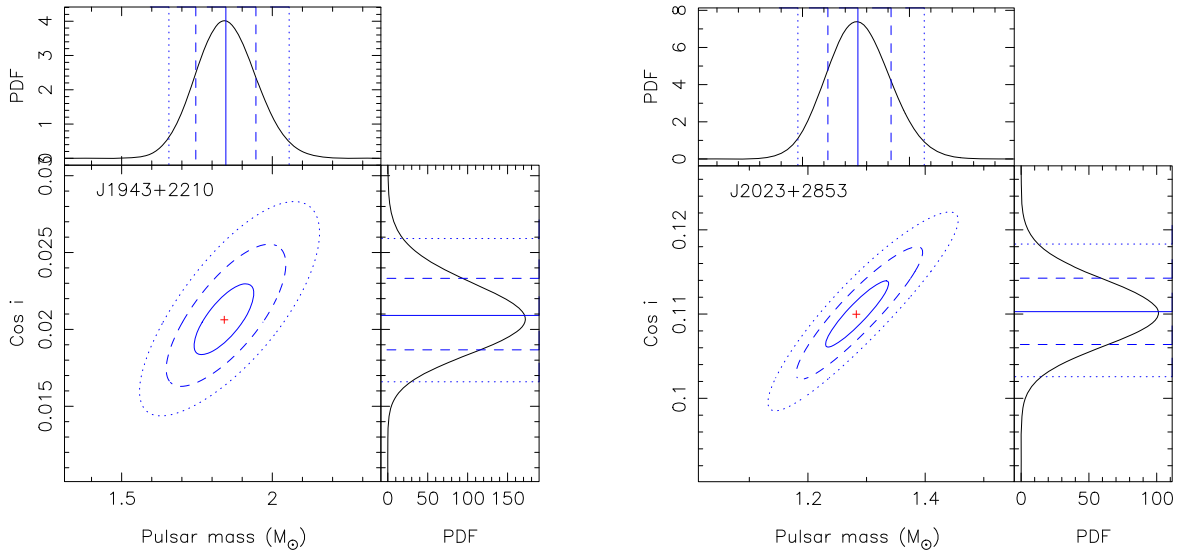

Figure 5. Constraints on the pulsar mass $m_{\rm p}$ and orbital inclination angle i for PSRs J1943+2210 and J2023+2853 by using the measured Shapiro delay. The contours in the main sub-panels show the likelihood in the two-dimensional probability distribution function (PDF) at the 39% ($\Delta\chi^2 = 1$), 86% ($\Delta\chi^2 = 4$), and 99% ($\Delta\chi^2 = 9$) confidence levels for the fitted ELL1k binary model. The red crosses indicate the best masses for the minimum χ^2. The one-dimensional PDFs for the $m_{\rm c}$ and $\cos i$ are shown in the upper and right sub-panels respectively with indications for the median, 1σ, and 2σ ranges.

$1.84^{+0.11}_{-0.09}$ $M_\odot$, one of the largest birth masses ever known (Tauris & van den Heuvel 2023). The measured companion mass is in the conjunction area between the CO WDs and ONeMg WDs, so it can be either a CO WD or an ONeMg WD.

Because of a relatively short orbital period and a high NS mass, this binary system has a coalescence time of 2.5 Gyr, the shortest among those IMBP systems with a recycled pulsar.

3.5. PSR J1947+2304

Using FAST observations of PSR J1947+2304 over more than 3 yr, we get the phase-connected timing solution of this binary pulsar. It has a spin period of 10.9 ms, and an orbital period of 0.339 days, with an eccentricity of a few 10^{-5}. The companion has a minimum companion mass of 0.87 $M_\odot$. We cannot get other constraints on the companion mass, and hence cannot determine the companion type as being a CO WD or an ONeMg WD.

Among all binary MSPs with a massive WD companion, the orbital period of PSR J1947+2304 is the shortest. Such a tight orbit could be the result of continuous gravitational wave emission over a long time if expressible by the pulsar characteristic age of 3.6 Gyr. General relativity predicts a variation rate of orbital period $\dot{P}_{\rm orb} \sim -1 \times 10^{-13}$, which should be measurable in the future. This binary system will merge within 3 Gyr due to gravitational wave emission.

3.6. PSR J2023+2853

PSR J2023+2853 is a very bright pulsar discovered in the FAST GPPS survey, which has been buried in the harmonics of

the nearby extremely bright pulsar PSR B2020+28 with a similar DM (Han et al. 2021). It has a spin period of 11.3 ms and is in a binary system with an orbital period of 0.72 days. Its pulse profile has an interpulse (see Figure 3), separated from the main pulse by 180° in the rotation longitude.

The orbit of PSR J2023+2853 is highly inclined, so the Shapiro delay can be very well detected and described using the PK parameters of $r \equiv 2Gm_c/c^3$ and $s \equiv \sin i$. On 2024 January 17th we launched a tracking observation for 3.5 hr by the FAST facility to cover the conjunction phase and a clear Shapiro delay was detected. When we drafted this paper, we noticed that the CHIME team published the timing results on the arXiv on 2024 February 13 for some bright pulsars with high cadences, including this bright pulsar (Tan et al. 2024). They obtained the two Shapiro delay parameters and calculated a companion mass of $0.93^{+0.17}_{-0.14}$ $M_\odot$ and a pulsar mass of $1.50^{+0.49}_{-0.38}$ $M_\odot$ (Tan et al. 2024).

The timing solutions we obtained by FAST are consistent with their published results but with much better precision. From the two PK parameters r and s we obtained $m_c = 0.85(2)$ $M_\odot$ and $\sin i = 0.9939(4)$. Because of the long span for timing and the better precision of measurements, we have also measured the proper motion of this pulsar as being 8.745(77) mas yr^{-1}. The parallax is 1.22(30) mas, which should be counted when used for a test of general relativity. The corresponding parallax distance is 0.8(0.2) kpc, closer than but still consistent with its DM distance estimate within 3σ uncertainty. All these measurements can constrain the masses of PSR J2023+2853 and its companion. We performed the Bayesian analysis of parameters, as displayed in Figure 5. We arrived at the pulsar mass m_p of $1.28^{+0.06}_{-0.05}$ $M_\odot$, the companion mass m_c of 0.853 ± 0.020 $M_\odot$, the total mass m_{tot} of $2.14^{+0.08}_{-0.07}$ $M_\odot$, and an orbital inclination i of $83.7^{+0.2}_{-0.3}$ deg. Similar results have been obtained using the DDGR model-fitting (Damour & Deruelle 1985, 1986), which gives the companion mass of 0.857 ± 0.018 $M_\odot$ and the total mass of 2.15 ± 0.07 $M_\odot$. According to the companion mass, its companion is a CO WD.

4. Discussions

These six compact IMBP systems should be products of CE evolution (Tauris et al. 2011, 2012; Tauris & van den Heuvel 2023). The mass accretion should cause the spin axis to be aligned with the orbital axis. These two compact objects with different masses can act as a laboratory to test gravitational theories. The precise timing of such systems can measure the pulsar masses which are the key parameters for understanding the evolution channels of NSs and are constraints for the equation of state of supra-nuclear matter (e.g., Horvath et al. 2021).

4.1. Possible Tests of Gravitational Theory with High Accuracy Data from PSRs J1943+2210 and J2023+2853

FAST measurements of PSRs J1943+2210 and J2023+2853 give an rms residual with a high precision of 7 and 0.5 μs respectively. Because of highly inclined orbits, the two Shapiro delay parameters have been used to constrain the companion masses, pulsar masses, and the inclination angles of the orbits. Their precise proper motions and the parallax of J2023+2853 are also measured from timing data, as shown above. The periastron advance ($\dot{\omega}$) and changes of orbital period $\dot{P}_{orb}$ are still not well measured, but their uncertainties will decrease with a longer observation span T by $T^{-3/2}$ and $T^{-5/2}$, respectively.

In some gravity theories, such as the scalar-tensor theories, the dipolar gravitational waves are predicted to radiate from an asymmetric binary system with significantly different masses with different gravitational self-energies, though not in general relativity. Binary MSPs with a WD companion indeed provide a unique opportunity for such a test (Freire et al. 2012; Guo et al. 2021; Gautam et al. 2022). The orbital period derivatives $\dot{P}_{orb}$ of PSRs J1943+2210 and J2023+2853 will be especially useful to constrain the spontaneous scalarization (Damour & Esposito-Farese 1993), as shown for the case of PSR J2222–0137 by Zhao et al. (2022). According to Cognard et al. (2017), for a binary orbit with a negligible eccentricity, the additional change rate of the orbital period in the scalar-tensor theories should be

$$|\alpha_p - \alpha_c|^2 = \delta\dot{P}^D_{orb}\left(\frac{P_{orb}}{4\pi^2}\right)\left(\frac{M_\odot}{T_\odot m_c}\right)\left(\frac{q+1}{q}\right), \quad (3)$$

where α_p and α_c are the scalar charge or effective coupling strength of the pulsar and its companion respectively, $\delta\dot{P}^D_{orb}$ is the orbital damping caused by dipolar gravitational wave emission, and q is the mass ratio m_p/m_c. Obviously the theoretical constraints for $|\alpha_p - \alpha_c|^2$ depend on the precision of $\delta\dot{P}^D_{orb}$. For PSR J1943+2210, if $\delta\dot{P}^D_{orb}$ can be constrained to be less than 4 fs s^{-1}, then $|\alpha_p - \alpha_c|$ can reach 1×10^{-3}. For PSR J2023+2853, if we can constrain $\delta\dot{P}^D_{orb}$ to be less than 1 fs s^{-1}, then $|\alpha_p - \alpha_c|$ should be smaller than 1×10^{-3}, better than the constraints from other systems, e.g., 1.9×10^{-3} for PSR J1738+0333 from Freire et al. (2012) and 3.3×10^{-3} for PSR J2222−0137 from Guo et al. (2021). We do need to observe it for a longer observation span T.

However, the observed excessive orbital period derivative may have other possible origins, as expressed by

$$\dot{P}^{ex}_{orb} = \delta\dot{P}^D_{orb} + \dot{P}^{Gal}_{orb} + \dot{P}^{shk}_{orb}, \quad (4)$$

here $\dot{P}^{Gal}_{orb}$ is the contribution of Galactic acceleration, and $\dot{P}^{shk}_{orb}$ is caused by the proper motion (Shklovskii 1970). Taking the distance from the Sun to the Galactic center as being 8.0 kpc and the Galactic circular velocity of 220 km s^{-1} at the location

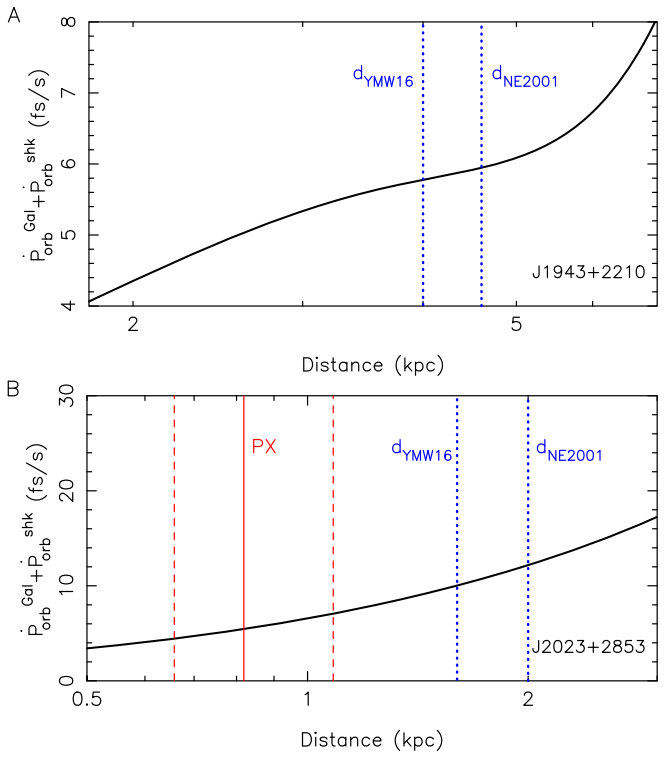

Figure 6. The sum of the predicated observed orbital decay due to the Galactic acceleration and the proper motion as a function of distance to the pulsar. The black line shows the variation of kinematic contribution to the $\dot{P}_{\rm orb}$ as a function of distance. The blue dotted lines indicate the estimated distances by using the Galactic electron-density models of NE2001 (Cordes & Lazio 2002) and YMW16 (Yao et al. 2017). The pulsar distance of PSR J2023+2853 has been derived from the timing parallax, with the 1σ uncertainty indicated by the vertical dashed lines.

of the Sun (GRAVITY Collaboration et al. 2019), we find that the sum of the two contributions is a function of distance, as illustrated in Figure 6.

At present, no reliable distance measurement for PSR J1943+2210 prevents an accurate assessment of kinematic effects and hence a good constraint on the dipolar gravitational wave emission (see Figure 6). Based on the parallax distance of PSR J2023+2853, the sum of the two contributions from Galactic acceleration and proper motion should be 4.4–7.1 fs s^{-1} in the 68% confidence level. In the future, with more data for more accurate measurements of parallax (for PSR J2023+2853), the Shapiro delay and proper motion, the two binary systems of PSRs J1943+2210 and J2023+2853 can potentially provide the best constraint on the existence of dipolar gravitational wave emission.

4.2. Two Possible Formation Channels of Compact IMBP Systems

If the WD companion was formed before the NS, the binary system should be in an eccentric orbit (Antoniadis et al. 2011), as indicated by the filled triangle in Figure 1. Otherwise, the orbits of the binary systems should be nearly circular (Tauris & van den Heuvel 2023).

All six IMBPs presented in this paper have circular orbits, therefore these systems probably descended from IMXBs with very wide orbits of $P_{\rm orb} \sim 10^2$–10^3 days. The companion star previously had a mass of 2–10 $M_\odot$, and it became a giant. Such a giant star responds to the mass loss by expanding, and then the mass transfer rate rises quickly, even far exceeding the mass accretion rate of the NS, then a CE is formed. The NS will spiral into the CE during which orbital momentum and the dynamic energy of the NS is then transferred into the CE. If the CE is successfully ejected in $\lesssim 10^3$ yr (Podsiadlowski 2001; Passy et al. 2012; Tauris et al. 2012), the outcome of this spiral-in phase should be a compact binary system consisting of an NS and a He star (Paczynski 1976; Iben & Livio 1993; Ivanova et al. 2013).

The accreted mass during the CE phase can recycle the NS to a spin period of $\sim$10 ms, with an amount of about 0.01 $M_\odot$. Conventionally, such spin periods should be reached in the post-CE mass accretion phase triggered by the Case BB RLO, during which the mass is transferred from a giant helium star to an NS, but it takes a much longer time of $\sim 10^5$ yr to get partially recycled (Tauris et al. 2011, 2012). Such a Case BB RLO evolution phase can only happen for those NS plus He star binaries with a tight orbit, in which the orbital energy of the progenitor is sufficient to fully eject the envelope of the donor star that evolves to near the tip of the red giant branch. A compact pulsar-helium star binary system should be left after the CE ejection. To avoid a merger, the orbital period should be $\lesssim$0.5 days (Tauris et al. 2011, 2012). After the Case BB RLO phase, a compact IMBP system with a mildly recycled pulsar should be formed.

Another possible formation channel for these compact IMBPs is the Case C channel, where the CE phase was initiated with an asymptotic giant branch star. Unlike the Case BB evolution channel, the helium core of the companion star has been exhausted, and the system will not go though Case BB RLO. The hypercritical accretion cooled by neutrino loss during CE phase (Houck & Chevalier 1991) or post-CE thermal remnant thermal readjustment phase (Ivanova 2011) may significantly spin up the NS, providing an alternative explanation to the mildly recycled pulsars. , To explain the heavy NS mass $1.84^{+0.11}_{-0.09}$ $M_\odot$ of PSR J1943+2210 that has a spin period of 12.9 ms, the accreted mass is about $\sim$0.01 $M_\odot$ according to Equation (14) in Tauris et al. (2012) in the recycling process, so the initial mass of PSR J1943+2210 should be about 1.83 $M_\odot$. It is a born-massive NS, similar to those in the systems of PSRs J1614−2230, PSR J1640+2224, PSR J2222−0137 and 2A 1822−371 (Tauris et al. 2011; Deng et al. 2020; Guo et al. 2021; Wei et al. 2023).

Such compact IMBP systems are rare. Previously only five MSPs with massive WD companions were located in compact orbits with a period less than 1 day (Edwards & Bailes 2001; Faulkner et al. 2004; Manchester et al. 2005; Ransom et al. 2005; Knispel et al. 2011; Ng et al. 2014), as listed in Table 1. We find six compact IMBPs with orbital periods less than 1 day, PSRs J0416+5201, J0520+3722, J1919+1341, J1943+2210, J1947+2304 and J2023+2853. Five of them will merge within a Hubble time except for the last one, making them the progenitors of Galactic gravitational wave sources for space-borne gravitational wave detectors like Tianqin (Luo et al. 2016), Taiji (Ruan et al. 2020), and LISA (Amaro-Seoane et al. 2017). Their tight orbits, relatively fast spin periods and the large companion masses are all consistent with the prediction of the Case BB RLO evolution channel (Tauris et al. 2011, 2012; Tauris & van den Heuvel 2023).

4.3. Geometry and Pulse Profile

During the Case BB RLO, the NS is spun up so that the rotation axis should get aligned with the orbital angular momentum (Yang & Li 2023). If so, and if the orbit is nearly edge-on, then our line of sight should be perpendicular to the pulsar spin axes. The Shapiro delay signals have been detected in PSRs J0416+5201, J0520+3722, J1943+2210 and J2023+2853, which is a clear indication for their edge-on orbits. The detected radio emission indicates that their magnetic field poles are aligned to our line of sight. If the surface magnetic fields of such a pulsar are dipolar, then the magnetic axis must be highly inclined from the spin axis. So, they are perpendicular rotators, from which an interpulse may be observed. Indeed, the pulsars PSRs J0416+5201, J0520+3722, J1943+2210 and J2023+2853 all have a pulse profile with two discrete pulses. Among them, an interpulse is observed approximately half-way through the spin cycle except for PSR J1943+2210.

PSRs J1913+1341 and J1947+2304 only have one pulse and no Shapiro delay signals have been detected yet. Their orbital inclinations are not constrained yet due to large TOA uncertainties.

Though the rotating vector model (Radhakrishnan & Cooke 1969) has been widely applied to normal pulsars, we tried to fit the model to PSRs J0520+3722, J1943+2210 and J2023+2853 and obtained large inclinations of magnetic axis from the rotation axis, see α and ζ in Figure 3. These results suggest that the NSs, i.e., the pulsars, have been spun up by a stable mass transfer process in, e.g., Case BB RLO (Tauris & van den Heuvel 2023) or post-CE thermal remnant thermal readjustment phase (Ivanova 2011). If the system was formed via the Case C channel and the NS was spun up via the neutrino- cooling accretion during the CE phase, the pulsar spin axis may be misaligned with the orbital orientation.

Among other known compact IMBPs, PSRs J1525−5545, J1757−5322 and J1748−2446N have only one on-pulse region and no constraint on their orbital inclination angles has been reported yet (Edwards & Bailes 2001; Ransom et al. 2005; Ng et al. 2014). PSRs J1802−2124 and J1952+2630 also have only one on-pulse region, and the orbital inclination of J1802 −2124 is 79.9(6) deg and that of J1952+2630 is ∼72 deg (Ferdman et al. 2010; Gautam et al. 2022). More detailed study of their geometry may help us to understand their origin.

Acknowledgments

We thank Dr Miquel Colom i Bernadich, Dr Paulo Freire and the two referees for their careful reading of the manuscript and helpful suggestions. This work made use of the data from FAST (Five-hundred-meter Aperture Spherical radio Telescope) (https://cstr.cn/31116.02.FAST). FAST is a Chinese national mega-science facility, operated by National Astronomical Observatories, Chinese Academy of Sciences. The GPPS survey project is one of five key projects of FAST. The authors are supported by the National Natural Science Foundation of China (NSFC, Grant Nos. 11988101, 12133004 and 11833009) and the Research Program of the Chinese Academy of Sciences (grant No. QYZDJ-SSW-SLH021 and JZHKYPT-2021-06).

Data Availability

Original FAST observational data will be an open resource according to the FAST data 1 yr protection policy. The folded and calibrated pulsar profiles presented in this paper can be found on the webpage: http://zmtt.bao.ac.cn/psr-fast/.

Authors Contributions

The FAST GPPS survey is a key FAST science project led by J. L. Han. He organized the teamwork for the survey and follow-up observations, processed the survey data, and discovered these pulsars. Timing data have been observed by P. F. Wang (via PT2023_0190), T. Wang (via PT2022_0159), W. Q. Su (via PT2021_0132), Chen Wang (via PT2023_0017), Z. L. Yang (via PT2023_0084 and PT2024_0200) and D. J. Zhou (via PT2023_0188). Z. L. Yang processed all data presented in this paper and drafted the manuscript under the supervision of J. L. Han. J. L. Han was finally in charge of finishing this paper. P. F. Wang developed the processing procedures for pulsar polarization profile and pulsar timing which are extensively used in this paper. Chen Wang feeds all targets for the GPPS observations. D. J. Zhou, Tao Wang, W. C. Jing, Y. Yan, Lang Xie and N. N. Cai contributed to different aspects of data processing and/or joined many group discussions. P. F. Wang and Jun Xu made fundamental contributions to the construction and maintenance of the computational platform. Other people jointly proposed or contributed to the FAST key project. All authors contributed to the finalization of this paper.

ORCID iDs

Z. L. Yang https://orcid.org/0009-0009-6590-1540
J. L. Han https://orcid.org/0000-0002-9274-3092
T. Wang https://orcid.org/0000-0002-4704-5340
P. F. Wang https://orcid.org/0000-0002-6437-0487
W. Q. Su https://orcid.org/0009-0003-2212-4792
D. J. Zhou https://orcid.org/0000-0002-6423-6106
Y. Yan https://orcid.org/0009-0008-1612-9948
W. C. Jing https://orcid.org/0000-0002-1056-5895

References

Alpar, M. A., Cheng, A. F., Ruderman, M. A., & Shaham, J. 1982, Natur, 300, 728
Amaro-Seoane, P., Audley, H., Babak, S., et al. 2017, arXiv:1702.00786
Antoniadis, J., Bassa, C. G., Wex, N., Kramer, M., & Napiwotzki, R. 2011, MNRAS, 412, 580
Berthereau, A., Guillemot, L., Freire, P. C. C., et al. 2023, A&A, 674, A71
Bhattacharya, D., & van den Heuvel, E. P. J. 1991, PhR, 203, 1
Bhattacharyya, B., & Nityananda, R. 2008, MNRAS, 387, 273
Chambers, K. C., Magnier, E. A., Metcalfe, N., et al. 2016, arXiv:1612.05560
Chen, X., Han, J. L., Su, W. Q., Yang, Z. L., & Zhou, D. J. 2023, RAA, 23, 104004
Cognard, I., Freire, P. C. C., Guillemot, L., et al. 2017, ApJ, 844, 128
Colom i Bernadich, M., Venkatraman Krishnan, V., Champion, D. J., et al. 2024, A&A, 690, A253
Cordes, J. M., & Lazio, T. J. W. 2002, arXiv: astro-ph/0207156
Damour, T., & Deruelle, N. 1985, AIHPA, 43, 107
Damour, T., & Deruelle, N. 1986, AIHPA, 44, 263
Damour, T., & Esposito-Farese, G. 1993, PhRvL, 70, 2220
Damour, T., & Taylor, J. H. 1992, PhRvD, 45, 1840
Deng, Z.-L., Gao, Z.-F., Li, X.-D., & Shao, Y. 2020, ApJ, 892, 4
Edwards, R. T., & Bailes, M. 2001, ApJL, 547, L37
Edwards, R. T., Hobbs, G. B., & Manchester, R. N. 2006, MNRAS, 372, 1549
Faulkner, A. J., Stairs, I. H., Kramer, M., et al. 2004, MNRAS, 355, 147
Ferdman, R. D., Stairs, I. H., Kramer, M., et al. 2010, ApJ, 711, 764
Freire, P. C., Kramer, M., & Lyne, A. G. 2001, MNRAS, 322, 885
Freire, P. C. C., & Ridolfi, A. 2018, MNRAS, 476, 4794
Freire, P. C. C., Wex, N., Esposito-Farèse, G., et al. 2012, MNRAS, 423, 3328
Gautam, T., Freire, P. C. C., Batrakov, A., et al. 2022, A&A, 668, A187
GRAVITY Collaboration, Abuter, R., Amorim, A., et al. 2019, A&A, 625, L10
Guo, Y. J., Freire, P. C. C., Guillemot, L., et al. 2021, A&A, 654, A16
Han, J. L., Wang, C., Wang, P. F., et al. 2021, RAA, 21, 107
Han, J. L., Zhou, D. J., Wang, C., et al. 2025, RAA, 25, 104001
Hobbs, G. B., Edwards, R. T., & Manchester, R. N. 2006, MNRAS, 369, 655
Horvath, J. E., Rocha, L. S., Bernardo, A., Valientim, R., & de Avellar, M. G. B. 2021, AN, 342, 294
Hotan, A. W., van Straten, W., & Manchester, R. N. 2004, PASA, 21, 302
Houck, J. C., & Chevalier, R. A. 1991, ApJ, 376, 234
Iben, I. J., & Livio, M. 1993, PASP, 105, 1373
Ivanova, N. 2011, ApJ, 730, 76
Ivanova, N., Justham, S., Chen, X., et al. 2013, A&ARv, 21, 59
Jang, J., Main, R., Venkatraman Krishnan, V., et al. 2024, A&A, 689, A296
Jiang, P., Tang, N.-Y., Hou, L.-G., et al. 2020, RAA, 20, 064
Knispel, B., Lazarus, P., Allen, B., et al. 2011, ApJL, 732, L1
Lange, C., Camilo, F., Wex, N., et al. 2001, MNRAS, 326, 274
Luo, J., Chen, L.-S., Duan, H.-Z., et al. 2016, CQGra, 33, 035010
Manchester, R. N., Hobbs, G. B., Teoh, A., & Hobbs, M. 2005, AJ, 129, 1993
Nan, R. 2006, ScChG, 49, 129
Nan, R., Li, D., Jin, C., et al. 2011, IJMPD, 20, 989
Ng, C., Bailes, M., Bates, S. D., et al. 2014, MNRAS, 439, 1865
Paczynski, B. 1976, in Structure and Evolution of Close Binary Systems, ed. P. Eggleton, S. Mitton, & J. Whelan, 73 (Cambridge: Cambridge Univ. Press), 75
Passy, J.-C., De Marco, O., Fryer, C. L., et al. 2012, ApJ, 744, 52
Podsiadlowski, P. 2001, in ASP Conf. Ser. 229, Evolution of Binary and Multiple Star Systems, ed. P. Podsiadlowski et al. (San Francisco, CA: ASP), 239
Radhakrishnan, V., & Cooke, D. J. 1969, ApL, 3, 225
Radhakrishnan, V., & Srinivasan, G. 1982, CSci, 51, 1096
Ransom, S. M. 2001, PhD thesis, Harvard Univ., Massachusetts
Ransom, S. M., Hessels, J. W. T., Stairs, I. H., et al. 2005, Sci, 307, 892
Ruan, W.-H., Guo, Z.-K., Cai, R.-G., & Zhang, Y.-Z. 2020, IJMPA, 35, 2050075
Shamohammadi, M., Bailes, M., Flynn, C., et al. 2024, MNRAS, 530, 287–306
Shklovskii, I. S. 1970, SvA, 13, 562
Tan, C. M., Fonseca, E., Crowter, K., et al. 2024, ApJ, 966, 26
Tauris, T. M., Langer, N., & Kramer, M. 2011, MNRAS, 416, 2130
Tauris, T. M., Langer, N., & Kramer, M. 2012, MNRAS, 425, 1601
Tauris, T. M., & van den Heuvel, E. P. J. 2023, Physics of Binary Star Evolution. From Stars to X-ray Binaries and Gravitational Wave Sources (Princeton, NJ: Princeton Univ. Press)
van Kerkwijk, M. H., & Kulkarni, S. R. 1999, ApJL, 516, L25
van Straten, W., & Bailes, M. 2011, PASA, 28, 1
Wang, P. F., Han, J. L., Xu, J., et al. 2023, RAA, 23, 104002
Wang, P. F., Han, J. L., Yang, Z. L., et al. 2025, RAA, 25, 104003
Wei, N., Jiang, L., & Chen, W.-C. 2023, A&A, 679, A74
Yang, H.-r., & Li, X.-d. 2023, ApJ, 945, 2
Yao, J. M., Manchester, R. N., & Wang, N. 2017, ApJ, 835, 29
Zhao, J., Freire, P. C. C., Kramer, M., Shao, L., & Wex, N. 2022, CQGra, 39, 11LT01